# Crossed beam reaction of cyano radicals with hydrocarbon molecules. IV. Chemical dynamics of cyanoacetylene (HCCCN; $X\ ^1\Sigma^+$) formation from reaction of CN($X\ ^2\Sigma^+$) with acetylene, C$_2$H$_2$($X\ ^1\Sigma_g^+$)

L. C. L. Huang, O. Asvany,[a] A. H. H. Chang, N. Balucani,[b] S. H. Lin, Y. T. Lee, and R. I. Kaiser[c]

*Institute of Atomic and Molecular Sciences, 1, Section 4, Roosevelt Rd., 107 Taipei, Taiwan, Republic of China*

Y. Osamura[d]

*Department of Chemistry, Rikkyo University, 3-34-1 Nishi-ikebukuro, Toshima-ku, Tokyo, 171-8501, Japan*

The chemical reaction dynamics to form cyanoacetylene, HCCCN ($X\ ^1\Sigma^+$), via the radical–neutral reaction of cyano radicals, CN($X\ ^2\Sigma^+;\nu=0$), with acetylene, C$_2$H$_2$($X\ ^1\Sigma_g^+$), are unraveled in crossed molecular beam experiments at two collision energies of 21.1 and 27.0 kJ mol$^{-1}$. Laboratory angular distributions and time-of-flight spectra of the HCCCN product are recorded at $m/e=51$ and 50. Experiments were supplemented by electronic structure calculations on the doublet C$_3$H$_2$N potential energy surface and RRKM investigations. Forward-convolution fitting of the crossed beam data combined with our theoretical investigations shows that the reaction has no entrance barrier and is initiated by an attack of the CN radical to the $\pi$ electron density of the acetylene molecule to form a doublet cis/trans HCCHCN collision complex on the $^2A'$ surface via indirect reactive scattering dynamics. Here 85% of the collision complexes undergo C–H bond rupture through a tight transition state located 22 kJ mol$^{-1}$ above the cyanoacetylene, HCCCN ($X\ ^1\Sigma^+$) and H($^2S_{1/2}$) products (microchannel 1). To a minor amount (15%) trans HCCHCN shows a 1,2-H shift via a 177 kJ mol$^{-1}$ barrier to form a doublet H$_2$CCCN radical, which is 46 kJ mol$^{-1}$ more stable than the initial reaction intermediate (microchannel 2). The H$_2$CCCN complex decomposes via a rather loose exit transition state situated only 7 kJ mol$^{-1}$ above the reaction products HCCCN ($X\ ^1\Sigma^+$) and H($^2S_{1/2}$). In both cases the geometry of the exit transition states is reflected in the observed center-of-mass angular distributions showing a mild forward/sideways peaking. The explicit identification of the cyanoacetylene as the only reaction product represents a solid background for the title reaction to be included in reaction networks modeling the chemistry in dark, molecular clouds, outflow of dying carbon stars, hot molecular cores, as well as the atmosphere of hydrocarbon rich planets and satellites such as the Saturnian moon Titan. © *2000 American Institute of Physics.* [S0021-9606(00)01136-3]

## I. INTRODUCTION

Investigating the mechanisms to form distinct structural isomers in extraterrestrial environments is an important means to test chemical models on the evolution of cold (dark) molecular clouds. The HC$_3$N isomers cyanoacetylene, HCCCN, isocyanoacetylene, HCCNC, and HNCCC represent a particular problem as this system is the only known example of three structural isomers existing in the interstellar medium.[1] Among them the thermodynamically most stable HCCCN isomer has the largest abundance; both metastable HCCNC and HNCCC molecules were identified in the cold

molecular cloud TMC-1 and the outflow of the carbon star IRC+10126. A recent line survey toward the Taurus molecular cloud TMC-1 yielded abundance ratios of [HCCCN]:[HCCNC]:[HNCCC]=1000:8:1.[2] Although the number densities are well established, the formation mechanism of these isomers is far from being resolved. Ion–molecule reactions have been proposed in chemical models of the interstellar medium (ISM), but failed to reproduce the relative abundances.[3] Supported by electronic structure calculations, this model suggested a recombination of interstellar HCCCNH$^+$ ions with an electron from the cosmic radiation followed by an isomerization from HCCCNH to HCCNCH and H atom emission. However, this reaction sequence yields ratios of [HCCCN]:[HCCNC]:[HNCCC] =240:8:1. As a consequence, even though this mechanism can explain satisfactorily the abundances of both metastable isomers quantitatively, the majority of the HCCCN molecules cannot be produced via ion–molecule reactions.

It was therefore suggested that the bimolecular neutral–neutral reaction of the cyanogen radical, CN($X\ ^2\Sigma$), with acetylene, C$_2$H$_2$($X\ ^1\Sigma_g^+$), might produce cyanoacetylene in

[a] Also at the Department of Physics, Technical University Chemnitz, 09107 Chemnitz, Germany.

[b] Permanent address: Dipartimento di Chimica, Università di Perugia, 06123 Perugia, Italy.

[c] Also at the Department of Physics, Technical University Chemnitz, 09107 Chemnitz, Germany and Department of Physics, National Taiwan University, Taipei, 106, Taiwan, Republic of China. Electronic mail: kaiser@po.iams.sinica.edu.tw

[d] Author to whom correspondence should be addressed. Electronic mail: osamura@chem.rikkyo.ac.jp

TABLE I. Experimental beam conditions and $1\sigma$ errors: most probable velocity $v_p$, speed ratio $S$, most probable collision energy of the CN beam with the acetylene molecules, $E_{coll}$, and center-of-mass angles, $\theta_{CM}$.

| Experiment | $v_p$, m s$^{-1}$ | $S$ | $E_c$, kJ mol$^{-1}$ | $\Theta_{CM}$ |
|---|---|---|---|---|
| CN/C$_2$H$_2$ | $1560 \pm 30$ | $6.8 \pm 0.5$ | $21.1 \pm 0.7$ | $30.0 \pm 0.1$ |
| CN/C$_2$H$_2$ | $1828 \pm 20$ | $6.0 \pm 0.2$ | $27.0 \pm 0.4$ | $26.2 \pm 0.3$ |
| C$_2$H$_2$ | $900 \pm 15$ | $12.0 \pm 0.5$ | ... | ... |

the outflow of the circumstellar envelope surrounding the carbon star IRC+10216,[4] hot molecular cores,[5] and dark molecular clouds such as TMC-1:[6]

$$CN(X\,^2\Sigma^+) + C_2H_2(X\,^1\Sigma_g^+) \rightarrow HCCCN(X\,^1\Sigma^+) + H(^2S_{1/2}). \tag{1}$$
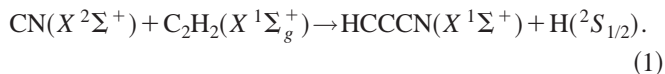
Recent laboratory measurements at ultralow temperatures as low as 20 K show that the reaction rate constant of (1) increases as the temperature decreases, reaching a maximum of $5 \times 10^{-10}$ cm$^3$ s$^{-1}$ at 30 K, i.e., in the order of gas phase collisions. However, these studies can monitor only the decay kinetics of the CN radical, and hence reaction products could not be determined explicitly.[7]

Investigation at the molecular level, where it is possible to observe the consequences of a single reactive event, can provide a direct insight into the reaction mechanism. We have recently reported[8] the first investigation of the title reaction by means of the crossed molecular beam (CMB) technique with mass spectrometric detection; the CN/H exchange channel was found to occur through the formation of a bound intermediate formed following the addition of a CN radical to the $\pi$ system of acetylene. Here, we report a more extensive investigation where the dependence of chemical reaction dynamics on the collision energy is also examined. In addition, the experimental results are complemented by the first complete *ab initio* molecular orbital calculations of the reaction potential energy surface, where all the possible reaction pathways were considered; the calculated geometry of the decomposing transition states allowed us to rationalize the observed preference for sideways scattering. The branching ratios among the possible reaction pathways were determined within the RRKM model.

## II. EXPERIMENT AND DATA ANALYSES

The experiments were performed with the 35 in. crossed molecular beams machine.[9] Briefly, a pulsed supersonic cyano radical beam, $CN(X\,^2\Sigma^+;\nu=0)$ in the vibrational ground state is generated *in situ* via laser ablation of graphite at 266 nm and seeding the ablated species in neat nitrogen carrier gas that acts as a reactant as well. The Spectra Physics GCR 270-30 Nd-YAG laser operates at 30 Hz and 30 mJ per pulse. A chopper wheel selects a segment of the CN beam, cf. Table I, which intersects a second, pulsed acetylene, C$_2$H$_2$, beam at 90° in the interaction region. Reactively scattered species are detected using a triply differentially pumped detector consisting of a Brink-type electron-impact ionizer, quadrupole mass filter, and a Daly ion detector[10] recording time-of-flight spectra (TOF) at different laboratory angles. Data accumulation times range up to 4 h at every

angle. Integrating these TOF spectra at different laboratory angles and correcting for the CN beam intensity drift yields the laboratory angular distribution (LAB). A forward-convolution technique is employed to gain information on the reaction dynamics from the laboratory data.[11] This approach assumes an angular flux $T(\theta)$ and a translational energy $P(E_T)$ trial distribution in the center-of-mass coordinate system assuming mutual independence. The final outcome is the generation of a velocity flux contour map $I(\theta,u)$ in the center-of-mass frame showing the intensity as a function of angle $\theta$ and velocity $u$. This plot contains all the basic information of the reactive scattering process.

## III. ELECTRONIC STRUCTURE AND RRKM CALCULATIONS

The potential energy surface (PES) of the reaction between C$_2$H$_2$ and the $CN(X\,^2\Sigma^+;\nu=0)$ radical has been investigated in terms of *ab initio* molecular orbital methods. We have employed the hybrid density functional B3LYP method, i.e., Becke's three-parameter nonlocal exchange functional[12] with the correlation functional of Lee, Yang, and Parr,[13] and the 6-311G$(d,p)$ basis set.[14] All computation has been carried out using the GAUSSIAN 98 program package.[15] The structures of the intermediates and transition states were confirmed with the vibrational analysis; all relative energies shown in this paper are the corrected values of the zero-point vibrational energies. The coupled cluster CCSD(T) calculations with the 6-311G$(d,p)$ basis set have also been performed for some of the critical structures in order to refine the energetics.[16]

According to the quasiequilibrium theory or RRKM theory,[17] the rate constant $k(E)$ at a collision energy $E$ for a unimolecular reaction $A^* \rightarrow A^\sharp \rightarrow P$ can be expressed as

$$k(E) = \frac{\sigma}{h} \cdot \frac{W^\#(E - E^\#)}{\rho(E)}, \tag{2}$$

where $\sigma$ is the symmetry factor, $W^\#(E - E^\#)$ denotes the total number of states of the transition state (activated complex) $A^\sharp$ with the barrier $E^\#, \rho(E)$ represents the density of states of the energized reactant molecule $A^*$, and $P$ is the product or products. The harmonic oscillator and rigid rotor approximation were assumed for the species involved throughout the rate constant calculations. The saddle point method was applied to evaluate $\rho(E)$ and $W(E)$.

## IV. RESULTS

### A. Reactive scattering signal

Reactive scattering signal was observed at $m/e = 51$ (C$_3$NH$^+$) and $50$ (C$_3$N$^+$); cf. Figs. 1–4. TOF spectra recorded at both mass-to-charge ratios show identical patterns revealing that the product of gross formula C$_3$NH is the only one formed from the reaction and that it fragments to the daughter ion with $m/e = 50$ in the electron impact ionizer. We did not observe any adduct at mass-to-charge ratio 52; this indicates that the lifetime of C$_2$H$_2$CN is too short to survive the flight from the collision region to the ionizer. Because of the high background level at $m/e = 27$, we were
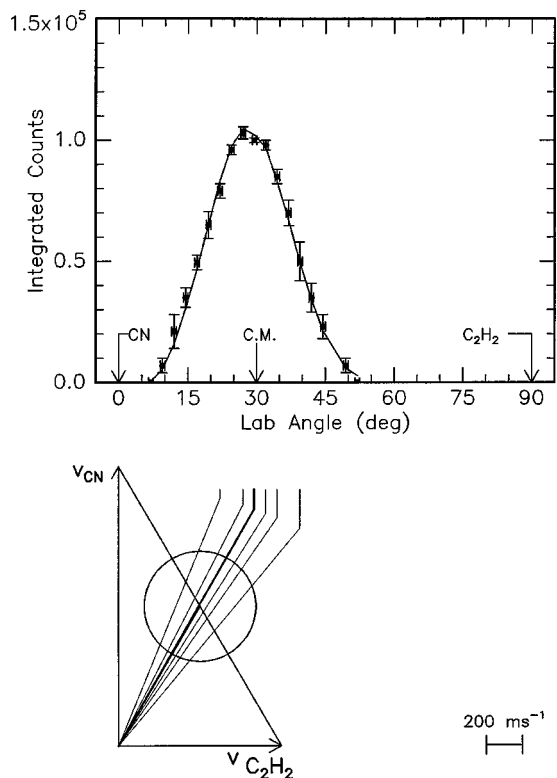
FIG. 1. Lower: Newton diagram for the reaction $CN(X\,{}^2\Sigma^+)$ $+\,C_2H_2(X\,{}^1\Sigma_g^+)$ at a collision energy of 21.1 kJ mol$^{-1}$. The circle delimits the maximum center-of-mass recoil velocity of the HCCCN product. Upper: Laboratory angular distribution of the HCCCN product at $m/e=50$. Circles and error bars indicate experimental data, the solid line the calculated distribution.
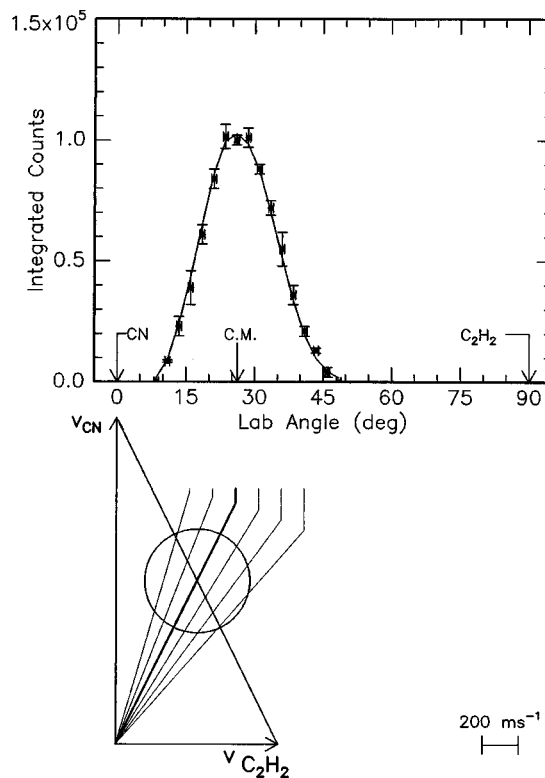
FIG. 2. Lower: Newton diagram for the reaction $CN(X\,{}^2\Sigma^+)$ $+\,C_2H_2(X\,{}^1\Sigma_g^+)$ at a collision energy of 27.0 kJ mol$^{-1}$. The circle delimits the maximum center-of-mass recoil velocity of the HCCCN product. Upper: Laboratory angular distribution of the HCCCN product at $m/e=50$. Circles and error bars indicate experimental data, the solid line the calculated distribution.

unable to detect a possible HCN or HNC reaction product from the H abstraction reaction to the ethynyl radical $C_2H$.

## B. Laboratory angular distributions (LAB) and TOF spectra

The most probable Newton diagrams of the reaction $CN(X\,{}^2\Sigma^+)+C_2H_2(X\,{}^1\Sigma_g^+)\rightarrow HCCCN(X\,{}^1\Sigma^+)+H({}^2S_{1/2})$ together with the laboratory product angular distributions are shown in Figs. 1 and 2 for the lower and higher collision energy, respectively. TOF spectra recorded at selected angles are depicted in Figs. 3 and 4. The solid lines superimposed on the experimental data are the calculated curves when employing the center-of-mass best-fit functions of Figs. 5 and 6. Both LAB distributions are slightly forward scattered with respect to the primary cyano radical beam and peak at 27.5° and 25.0° at lower and higher collision energy, respectively, that is close to the center-of-mass position angles of 30.0° and 26.2°. Both LAB distributions are very broad and spread over 40° and 50° in the scattering plane suggesting that the $P(E_T)$'s peak well away from zero. If we compare these scattering ranges with limiting Newton circles of the possible $C_3HN$ isomers, it is obvious that the thermodynamically most stable cyanoacetylene isomer, $HCCCN(X\,{}^1\Sigma^+)$, is mainly formed.

## C. Center-of-mass translational energy distributions, $P(E_T)$

Figures 5 and 6 depict the best-fit center-of-mass translational energy distribution functions within our experimental error limits. All $P(E_T)$'s peak between 20 and 30 kJ mol$^{-1}$, suggesting that the exit transition state from the decomposing $C_3H_2N$ intermediate to the reaction products is likely to be tight, involving a repulsive bond rupture and a significant electron reorganization. The best fit $P(E_T)$ energy tails extend up to an energy maximum $E_{max}$ of 100–132 kJ mol$^{-1}$ (Fig. 5) and 100–123 kJ mol$^{-1}$ (Fig. 6). The fits of the laboratory data do not change if the $P(E_T)$'s are extended or shortened by 10 kJ mol$^{-1}$. If we account for the collision energies, we find that the reaction is exothermic by about $90\pm10$ kJ mol$^{-1}$. Comparing this data with the exothermicities based on our electronic structure calculations (94 kJ mol$^{-1}$), shows that the thermodynamically most stable cyanoacetylene isomer is formed; cf. Sec. V. The thermodynamically unfavorable isocyanoacetylene isomer, HCCNC, is less stable by 107 kJ mol$^{-1}$ and therefore its formation is not consistent with the experimental findings. Finally, the fraction of total available energy channeling into translational energy of the products has been calculated: by assuming HCCCN as the only reaction product, we find fractions of 33%–36% almost independent on the collision energy.

J. Chem. Phys., Vol. 113, No. 19, 15 November 2000

Reaction of cyano radicals. IV    8659

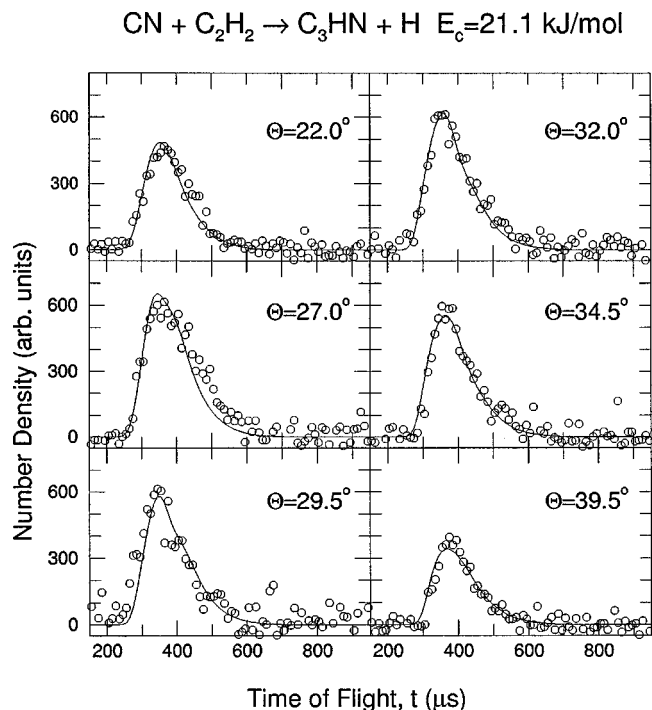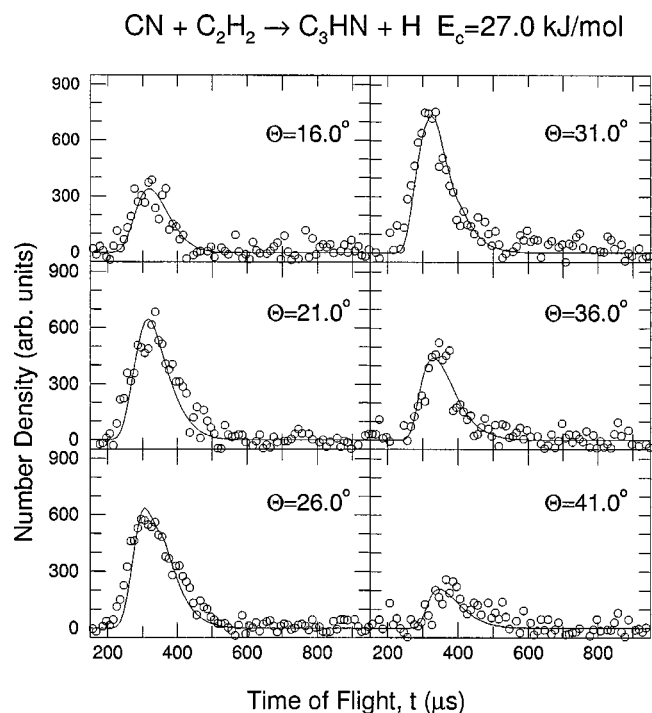## CN + C$_2$H$_2$ → C$_3$HN + H  E$_c$=21.1 kJ/mol



FIG. 3. Time-of-flight data of selected laboratory angles as indicated in Fig. 1. The dots indicate the experimental data, the solid lines the calculated fit.

This data is similar to complex forming reactions of atomic carbon and cyano radicals with unsaturated hydrocarbons, as studied earlier in our group.[18]

### D. Center-of-mass angular distributions, $T(\theta)$, and flux contour maps, $I(\theta,u)$

All $T(\theta)$'s and $I(\theta,u)$'s are forward–backward asymmetric and show intensity ratios at the poles of

## CN + C$_3$H$_2$ → C$_3$HN + H  E$_c$=27.0 kJ/mol



FIG. 4. Time-of-flight data of selected laboratory angles as indicated in Fig. 2. The dots indicate the experimental data, the solid lines the calculated fit.
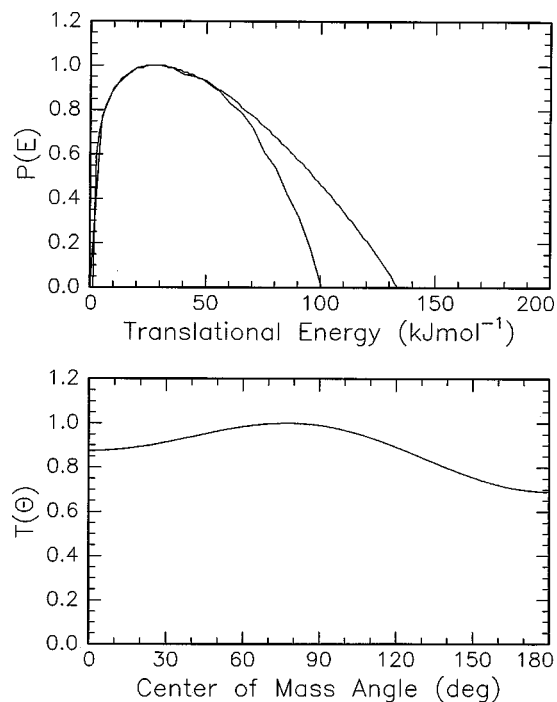


FIG. 5. Lower: Center-of-mass angular flux distribution for the reaction $CN(X\,^2\Sigma^+)+C_2H_2(X\,^1\Sigma_g^+)$ at a collision energy of 21.1 kJ mol$^{-1}$. Upper: Center-of-mass translational energy flux distribution for the reaction $CN(X\,^2\Sigma^+)+C_2H_2(X\,^1\Sigma_g^+)$ at a collision energy of 21.1 kJ mol$^{-1}$.

$I(0°)/I(180°)=1.24$ at lower and $I(0°)/I(180°)=1.17$ at higher collision energy, respectively; cf. Figs. 5–8. The product intensity observed in the whole angular range suggests that the reaction follows indirect scattering dynamics
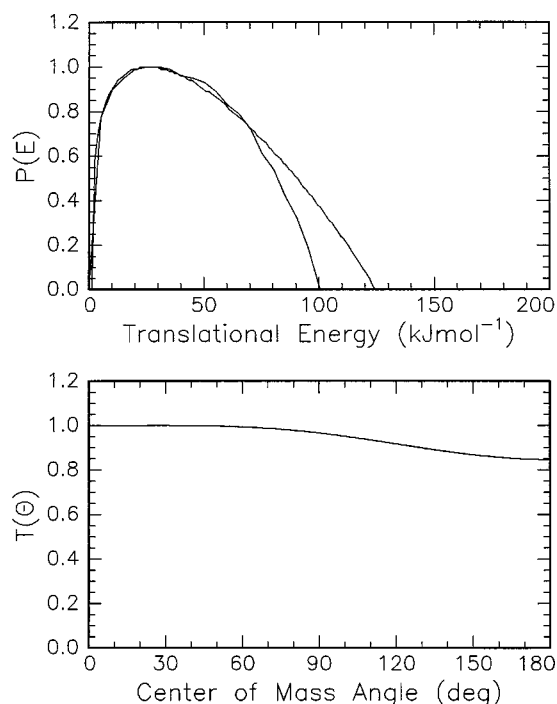


FIG. 6. Lower: Center-of-mass angular flux distribution for the reaction $CN(X\,^2\Sigma^+)+C_2H_2(X\,^1\Sigma_g^+)$ at a collision energy of 27.0 kJ mol$^{-1}$. Upper: Center-of-mass translational energy flux distribution for the reaction $CN(X\,^2\Sigma^+)+C_2H_2(X\,^1\Sigma_g^+)$ at a collision energy of 27.0 kJ mol$^{-1}$.
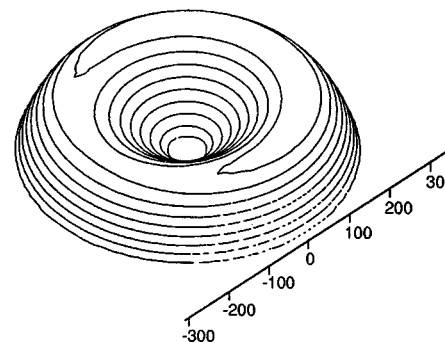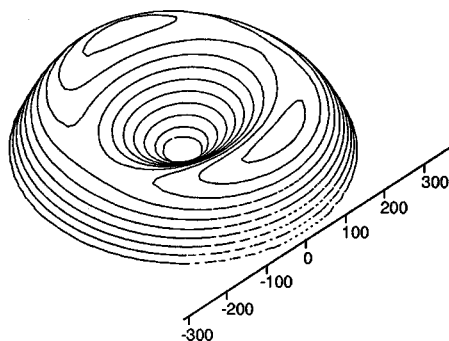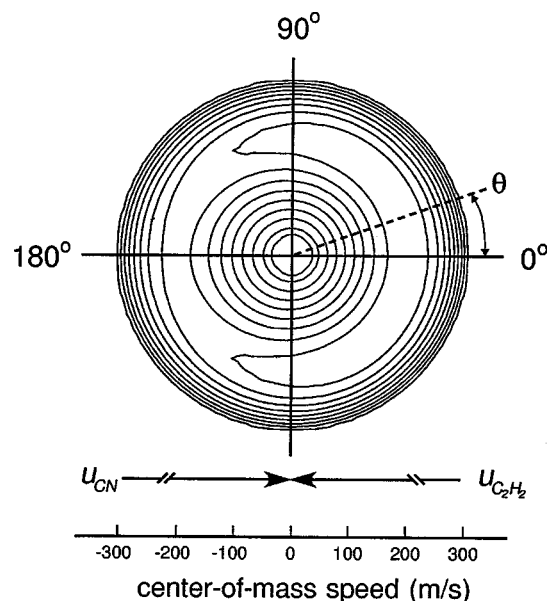
FIG. 7. Center-of-mass velocity contour flux map distribution for reaction $CN(X\,^2\Sigma^+) + C_2H_2(X\,^1\Sigma_g^+)$ at a collision energy of 21.1 kJ mol$^{-1}$. Units are given in m s$^{-1}$.
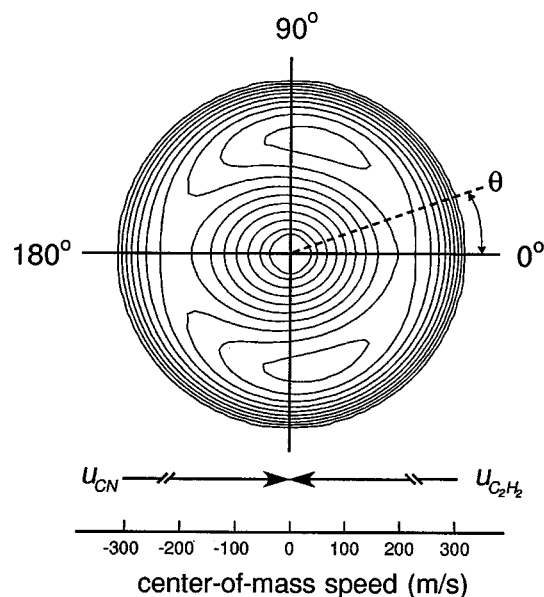
FIG. 8. Center-of-mass velocity contour flux map distribution for reaction $CN(X\,^2\Sigma^+) + C_2H_2(X\,^1\Sigma_g^+)$ at a collision energy of 27.0 kJ mol$^{-1}$. Units are given in m s$^{-1}$.

via a $C_3H_2N$ complex formation; the scattering preference for the forward (with respect to the CN beam direction taken as $\theta = 0°$) hemisphere implies that the complex lifetime is comparable to its rotational period, according to the osculating complex model of a chemical reaction. At lower collision energy, the $T(\theta)$ peaks on a broad plateau between $60°$ and $95°$, reflecting a ''bent displacement'' [19] of the light H atom during complex decomposition; cf. Sec. V. At the higher collision energy of 27.0 kJ mol$^{-1}$, the peak moves toward $\theta = 0°$ (see below).

## V. DISCUSSION

### A. *Ab initio* $C_3H_2N$ and $C_3HN$ potential energy surfaces (PES)

Electronic structure calculations help a great deal in unraveling the underlying chemical reaction dynamics of polyatomic neutral–neutral reactions. Therefore, we investigated computationally the reaction of the cyano radical, CN $(X\,^2\Sigma^+)$ with the acetylene molecule, $C_2H_2$ $(X\,^1\Sigma_g^+)$. This investigation is the first complete computation of the $C_3H_2N$ PES compared to previous studies.[20] Since the unpaired electron is localized in the $^2\Sigma^+$ orbital of the carbon atom, CN

attacks the $\pi_x / \pi_y$ orbital of the acetylene molecule barrier-less via a loose transition state. This process forms a deeply bound (242 kJ mol$^{-1}$) $C_s$ symmetric cis 1-cyanovinyl-2 radical intermediate, HCCHCN (int1c) on the $^2A'$ surface; cf. Figs. 9–11. Beside the cis structure, int1 exists in an isoenergetic trans form as well (int1t). Both the cis and trans forms of int1 can isomerize easily via TS1a located only 14 kJ mol$^{-1}$ above the initial collision complexes; since the isomerization barrier lies well below the total available energy, int1t and int1c are expected to be present in equal amounts. Alternatively, the CN radical can attack the acetylene molecule with its N side. Similarly to the reaction of the cyano radical with ethylene, the potential energy surface has no entrance barrier, and there is no transition state for the formation of a stable (148 and 147 kJ mol$^{-1}$) cis or trans 1-isocyanovinyl-2 intermediate, HCCHNC (nc-int1c/nc-int1t). In strong analogy to int1t/int1c, the isomerization barrier is only about 12/11 kJ mol$^{-1}$, and hence the ratio of nc-int1t to nc-int1c is anticipated to be unity. The initially formed isomer pairs int1c and nc-int1c as well as int1t and nc-int1t can isomerize via three-membered cyclic transition states TS1c and TS1t located 1 and 7 kJ mol$^{-1}$ slightly below the energy of both separated reactants; Figs. 9 and 12. A
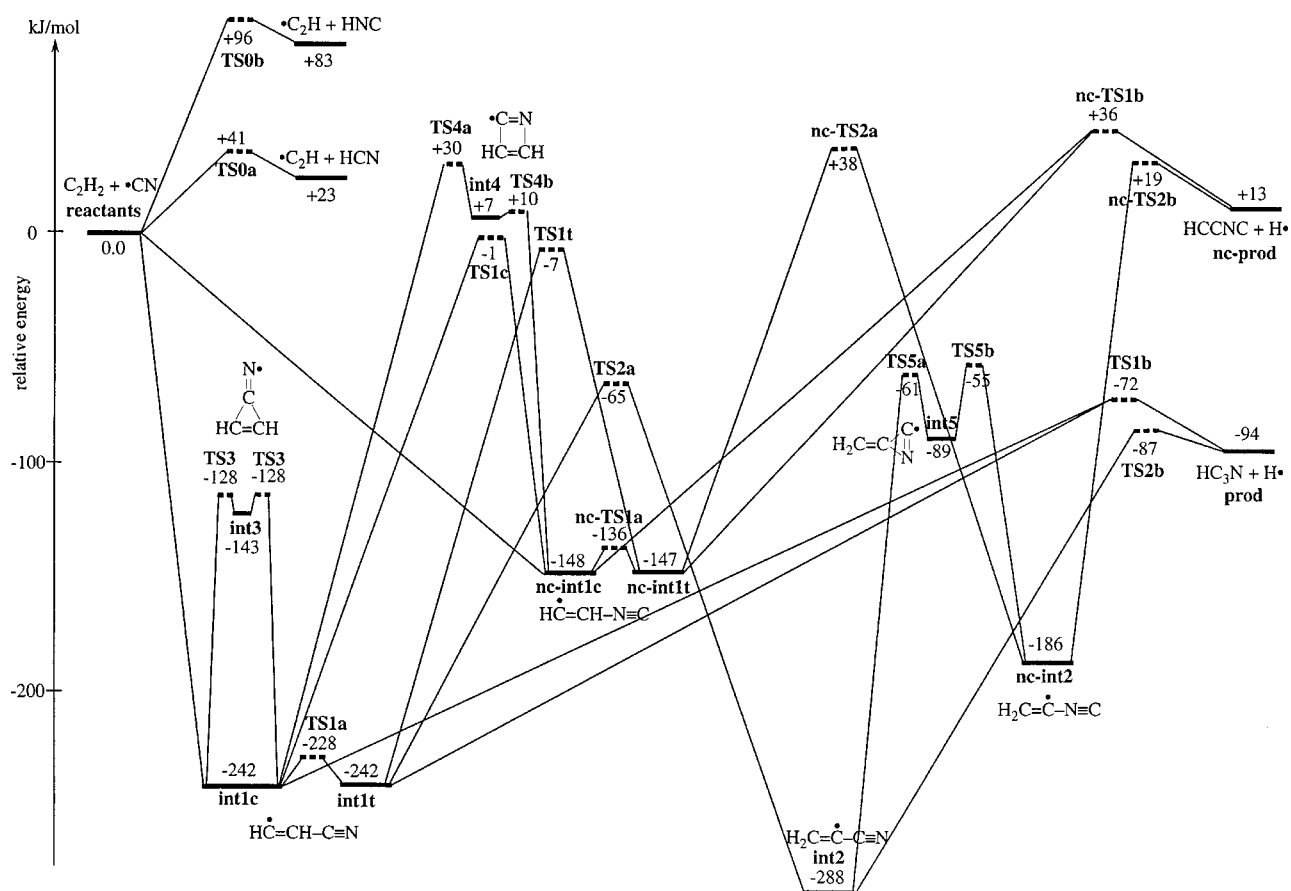
FIG. 9. Schematic representation of the C$_3$H$_2$N potential energy surface.

higher-energy isomerization process implies the formation of a bound, tetracyclic intermediate int4 via TS4b and TS4a. Both transition states together with the tetracyclic intermediate are higher in energy than the separated reactants. We like to point out that a ring closure of int1c via TS3 yields a loosely bound (15 kJ mol$^{-1}$) tricyclic intermediate int3. Since a H atom loss leads to a highly unstable (+357 kJ mol$^{-1}$) triplet $c$-C$_3$HN radical (prod3, Fig. 13), the only decay pathway of int3 is a ring opening to int1c, hence a migration of the CN group along the carbon–carbon skeleton of int1c. A CN group migration exists in nc-int1c as well; however, the resulting cyclic structure is found to be a first-order transition state, but not a bound reaction intermediate.

The C$_3$H$_2$N intermediates int1c/int1t and nc-int1c/nc-int1t can undergo either a H atom elimination to form cyanoacetylene or isocyanoacetylene or depict a 1,2 H atom shift. The decay pathways involve tight exit transition states located 22 kJ mol$^{-1}$ (TS1b) and 23 kJ mol$^{-1}$ (nc-TS1b) above the reaction products in exothermic (−94 kJ mol$^{-1}$) and endothermic (+13 kJ mol$^{-1}$) reactions. In both transition states, the H atom leaves along a direction forming an angle of about 90° with respect to the principal rotation axis A; cf. Figs. 10–11 and Fig. 15. The alternative 1,2 H atom shifts via TS2a and nc-TS2a result in int2 and nc-int2 that are stabilized by 288 and 186 kJ mol$^{-1}$. Although the barriers of both H atom shifts are of the same order of magnitude of about 180 kJ mol$^{-1}$, nc-TS2a does not play a role in our experiments since its energy of 38 kJ mol$^{-1}$ is higher than

the maximum collision energy of 27.0 kJ mol$^{-1}$. A weakly bound (about 30–35 kJ mol$^{-1}$) tricyclic intermediate int5 connects isomers int2 and nc-int2 via transition states TS5a and TS5b. Both int2 and nc-int2 can decay via a final carbon–hydrogen bond rupture through rather loose exit transition states TS2b and nc-TS2b located about 6–7 kJ mol$^{-1}$ above the products. The calculated structures of the two transition states indicate that their geometries are very close to the product structures and that the H atom is departing along a direction forming an angle of about 74° with respect to the principal rotation axis A; cf. Figs. 10–11 and Fig. 15.

A high-energy singlet cyanovinylidene vin1 (+115 kJ mol$^{-1}$) and singlet isocyanovinylidene nc-vin1 (+227 kJ mol$^{-1}$) isomers also exist; cf. Fig. 13. Both singlet species are formed without an exit barrier; the corresponding triplet carbenes vin3 and nc-vin3 are even higher in energy. Since our maximum collision energy is limited to 27 kJ mol$^{-1}$, none of the vinylidenes is relevant to our experiments. Finally, a H atom abstraction to form HCN or HNC is endothermic by 23 and 83 kJ mol$^{-1}$, respectively, and involves transition states located 41 and 96 kJ mol$^{-1}$ above the reactants (Fig. 14).

## B. Energetical considerations and RRKM calculations

The maximum translational energy releases of both $P(E_T)$ graphs are in line with a preferential formation of the
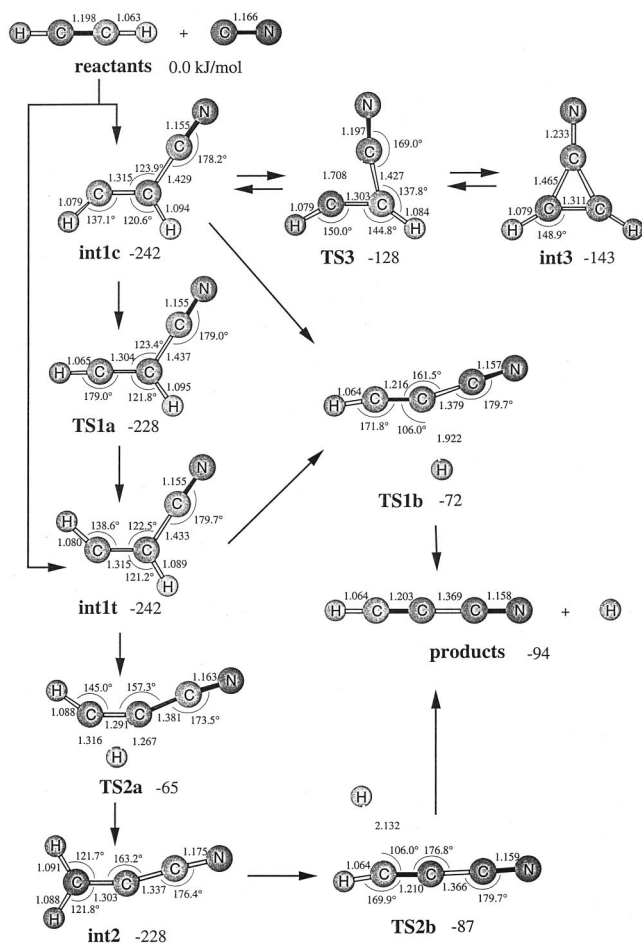
FIG. 10. Selected bond distances in angstroms and bond angles in degrees of reactants, intermediates, and transition states involved in the formation of cyanoacetylene.
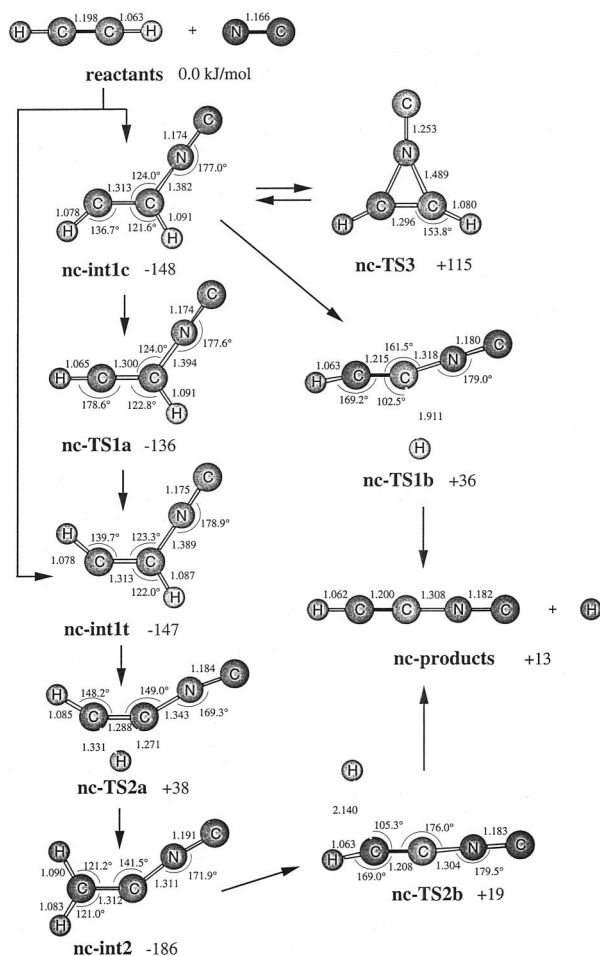
FIG. 11. Selected bond distances in angstroms and bond angles in degrees of reactants, intermediates, and transition states involved in the formation of isocyanoacetylene.

thermodynamically most stable cyanoacetylene isomer HCCCN in its $X\,^1\Sigma^+$ electronic ground state. Here, our best fits yield an exothermicity of $90 \pm 10\,\text{kJ mol}^{-1}$, whereas the electronic structure calculations show $94\,\text{kJ mol}^{-1}$. Based on published enthalpies of formations of the reactants and products, we calculate a reaction enthalpy of $-89.7\,\text{kJ mol}^{-1}$.[21] The formation of the second most stable isomer isocyanoacetylene, HCCNC, is endothermic by $13\,\text{kJ mol}^{-1}$, and hence cannot account for the majority of the reactive scattering signal. The involved potential energy surface verifies this conclusion. The formation of HCCNC must proceed either via nc-TS2b or nc-TS1b. The latter lies $36.0\,\text{kJ mol}^{-1}$ above the energy of the separated reactants; since the highest collision energy in our crossed beam experiments was $27.0\,\text{kJ mol}^{-1}$, this barrier could not be passed. Therefore, if HCCNC is a minor reaction product, nc-int2 is expected to decompose via nc-TS2b. Two pathways can lead to nc-TS2b: from intermediate nc-int1t via nc-TS2a or from int2 via TS5a, int5, and TS5b. Considering our maximum collision energy of $27.0\,\text{kJ mol}^{-1}$, nc-TS2a cannot be passed, and a cyano–isocyano isomerization from int2 to nc-int2 is the only remaining pathway. Our experimental data alone cannot quantify the contribution of the HCCNC isomer, and we employ RRKM calculations to tackle this problem. The rate equations for the title reaction were solved with the rate con-

stants computed by the RRKM theory; cf. Table II. As a result, the concentration of each species present in the reaction mechanism was obtained as a function of time. The concentration of the products at $t \rightarrow \infty$ were then taken to calculate the branching ratios.[22] This procedure shows that HCCCN is the sole reaction product. Even if nc-int1c and nc-int1t are formed as initial collision complexes, they react via TS1t and TS1c to int1c and int1t. Finally, we would like to point out that the formation of other $C_3HN$ isomers $c$-$C_3HN$ and the vinylidenes is not feasible since these reactions are too endothermic to be covered energetically. In addition, the barriers of H atom abstraction by CN to form either HCN or HNC is higher than the maximum collision energy employed in our experiments. Therefore we conclude that cyanoacetylene, HCCCN, is the sole reaction product.

## C. The actual reaction pathway

Our investigation shows that the title reaction follows indirect (complex forming) reactive scattering dynamics. The $CN(X\,^2\Sigma^+)$ radical attacks the $\pi_x/\pi_y$ orbital of the acetylene molecule barrierless via a loose transition state located at the centrifugal barrier to yield a $C_s$ symmetric trans or cis 1-cyanovinyl-2 radical intermediate, HCCHCN (int1t/int1c) on the $^2A'$ surface. The electronic structure calculations
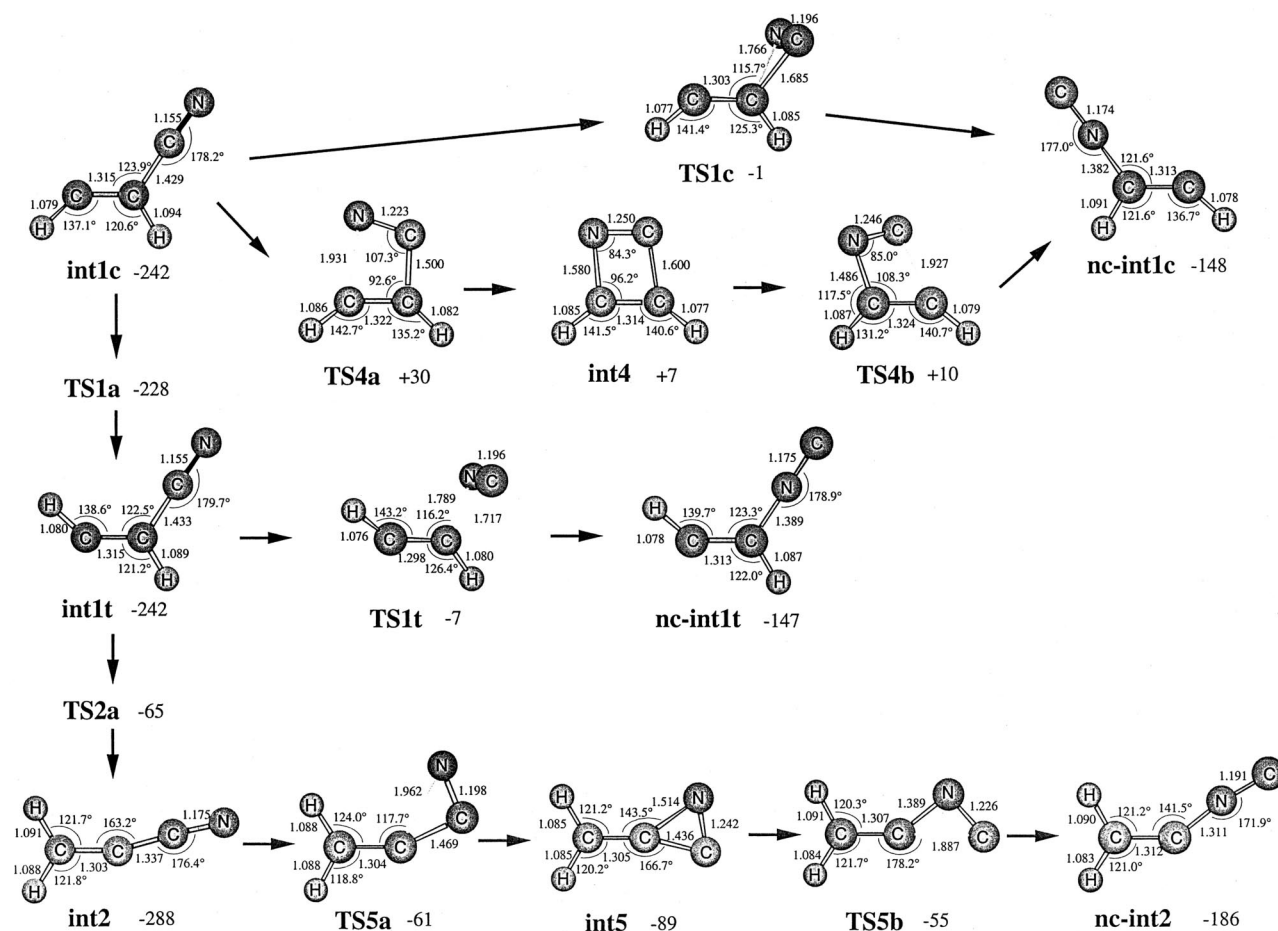
FIG. 12. Bond distances in angstroms and bond angles in degrees of intermediates and transition states involved in the $C_2H_2CN$–$C_2H_2NC$ isomerization.

show that both intermediates are stabilized by 242 kJ mol$^{-1}$ with respect to the reactants. The ultrafast cis-trans isomerization rate constant of $k=(2.64-2.80)\times 10^{13}\,s^{-1}$ verifies that int1t and int1c are present in equal concentrations. Upon complex formation, all four heavy atoms are rotating in a plane almost perpendicular to the total angular momentum vector **J** around the C axis of int1t/int1c. Both complexes can react via two microchannels, i.e., a decay via a carbon–hydrogen bond rupture through a tight transition state TS1b located 22 kJ mol$^{-1}$ above the HCCCN and H products (pathway 1) or a 1,2 H shift from int1t via TS2a to int2 prior to a H atom loss via a rather loose TS2b to HCCCN and H (pathway 2); the anisotropic exit potential excited the linear HCCCN molecules to B-like rotations. Our RRKM calculations quantify the branching ratio of microchannel 1 versus microchannel 2 to 85:15; this ratio is invariant as the collision energy varies from 0 to 30 kJ mol$^{-1}$.

The shape of the center-of-mass angular distributions can be understood within the framework of the microcanonical theory of angular distributions of reactive scattering proposed by the late Roger Grice.[18] Grice and Smith successfully applied this theory to the reaction OH+CO→$CO_2$+H, where the decomposing transition state approximates a linear rotor. In that case, the best fit of the experimentally determined center-of-mass angular distribution[23] was obtained by using a nominal preferred value of $\beta=45°$, where $\beta$ is the

angle between the dissociation direction and the principal inertia axis, A. The authors also displayed the resulting center-of-mass angular distributions when the angle $\beta$ shifts toward collinear configuration or toward more bent sideways configurations. For a similar prolate decomposing complex, dissociation along the B axis ($\beta=90°$) gives a sideways peaked center-of-mass angular distribution. The relevant decomposing transition states of our system can approximately be considered linear rotor; moreover, they encounter the criteria suggested by Grice for a reliable application of the model, that is the departing moiety is the light hydrogen atom and an exit potential energy barrier is associated to them. A closer inspection of the geometry of the two possible transition states TS1b and TS2b might suggest that TS1b is actually responsible for the sideways peaking observed at the lower collision energy; cf. Fig. 15. Indeed, the structure of TS2b should give a double peak in the center-of-mass angular distribution or, since a range of $\beta$ is actually possible, a large plateau from about $\theta=70°$ to $\theta=110°$. The geometry of TS1b, instead, is such that both $\theta=\beta$ and $\theta=180°-\beta$ give sideways scattering centered at about 90°. As a matter of fact, the lower $E_c$ center-of-mass angular distribution is peaked between 60° and 95° rather than around 90°, while the higher $E_c$ one is mildly peaked at $\theta=0°$. The peak shift toward $\theta=0°$, which augments as the available energy increases, may be taken as evidence that the
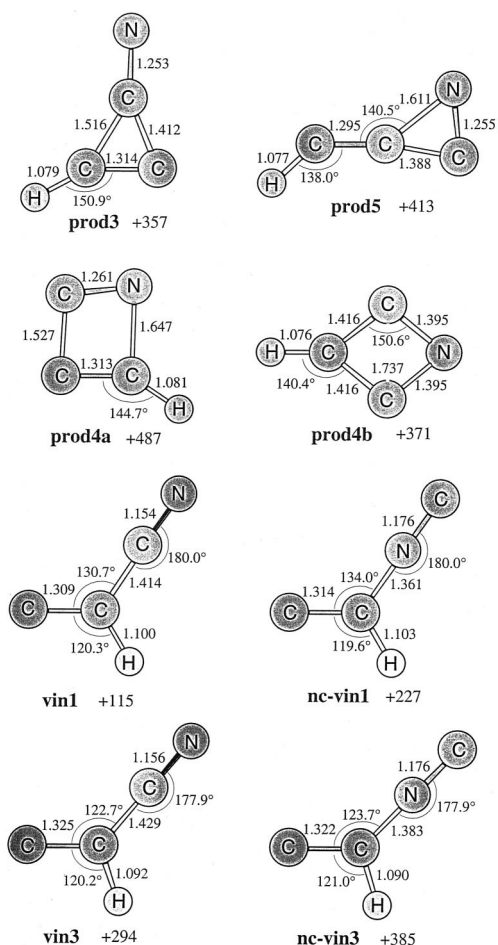
FIG. 13. Bond distances in angstroms and bond angles in degrees of cyclic C₃HN isomers together with cyanovinylidenes and isocyanovinylidenes. Relative energies with respect to the separated reactants are given in kJ mol$^{-1}$.
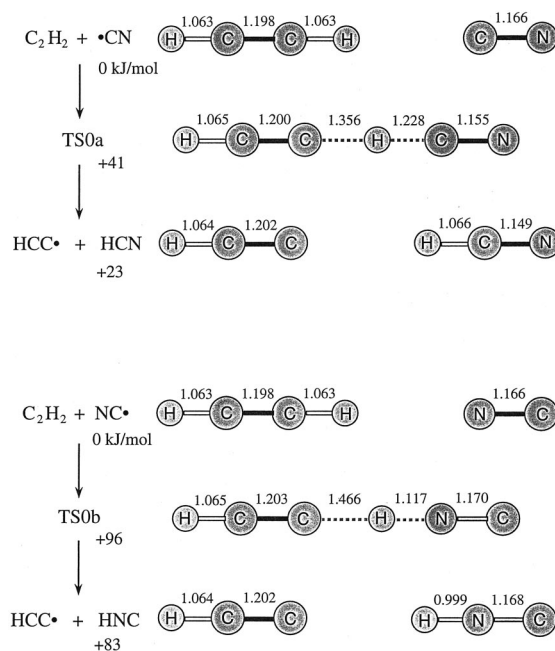


FIG. 14. Bond distances in angstroms of H atom abstraction channels to HCN and HNC.

are either endothermic or are inhibited due to an energetically not accessible exit barrier. Since the formation of HC-CCN has no entrance barrier, is exothermic, and all involved transition states are located well below the energy of the separated reactants, cyanoacetylene can be formed in very low temperature extraterrestrial environments such as cold molecular clouds TMC-1 holding average translational tem-

complex lifetime is actually a fraction of (or comparable to) the rotational period of the complex, according to the osculating model of chemical reaction. The further shift toward $\theta = 0°$ for the higher $E_c$ experiment could be interpreted both as (a) coming from a shortening of the complex lifetime or (b) a partial quenching of the reaction channel going through TS1b (pathway 1) in favor of the one going through TS2b (pathway 2), which would proceed through the formation of an osculating complex as well. The latter explanation can actually be disregarded since RRKM calculations have shown that the branching ratio between pathway 1 and 2 is invariant with collision energy.

## VI. IMPLICATIONS TO INTERSTELLAR AND SOLAR SYSTEM CHEMISTRY

Our crossed beam experiments together with *ab initio* and RRKM calculations verified for the first time explicitly that cyanoacetylene, HCCCN, is the sole reaction product of the radical–neutral reaction between an acetylene molecule, C₂H₂, and a cyano radical, CN($X\,^2\Sigma^+$) at relative collision energies of 21.1 and 27.0 kJ mol$^{-1}$. Neither the isocyano-acetylene isomer, HCCNC, nor the hydrogen abstraction products HCN or HNC were formed since these processes
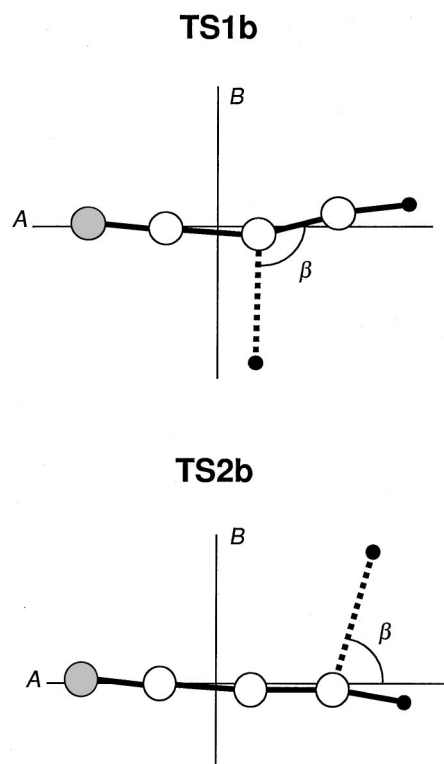


FIG. 15. Geometry of the exit transition states TS1b and TS2b together with the principal rotational axis. The C axis is perpendicular to the paper plane.

TABLE II. RRKM rate constants in $s^{-1}$ at two collision energies.

| Collision energy | $21.1 \text{ kJ mol}^{-1}$ | $27.0 \text{ kJ mol}^{-1}$ |
|---|---|---|
| $k(\text{int1c}\rightarrow\text{int1t})$ | $2.76\times10^{13}$ | $2.80\times10^{13}$ |
| $k(\text{int1t}\rightarrow\text{int1c})$ | $2.64\times10^{13}$ | $2.67\times10^{13}$ |
| $k(\text{int1t}\rightarrow\text{int2})$ | $1.62\times10^{10}$ | $2.25\times10^{10}$ |
| $k(\text{int2}\rightarrow\text{int1t})$ | $3.22\times10^{9}$ | $4.58\times10^{9}$ |
| $k(\text{int1c}\rightarrow\text{int3})$ | $1.88\times10^{11}$ | $4.52\times10^{11}$ |
| $k(\text{int3}\rightarrow\text{int1c})$ | $8.21\times10^{13}$ | $1.79\times10^{14}$ |
| $k(\text{int1c}\rightarrow\text{HCCCN}+\text{H})$ | $4.39\times10^{10}$ | $6.01\times10^{10}$ |
| $k(\text{int1t}\rightarrow\text{HCCCN}+\text{H})$ | $4.20\times10^{10}$ | $5.75\times10^{10}$ |
| $k(\text{int2}\rightarrow\text{HCCCN}+\text{H})$ | $4.58\times10^{10}$ | $6.09\times10^{10}$ |
| $k(\text{nc-int2}\rightarrow\text{HCCCN}+\text{H})$ | $2.04\times10^{4}$ | $8.34\times10^{5}$ |

peratures as low as 10 K and the atmosphere of Saturn's moon Titan. Likewise, this mechanism can account for the formation of the HCCCN isomer in ultracompact HII regions.[24] Therefore, the title reaction can be identified as the missing source of interstellar cyanoacetylene molecules that cannot be formed via postulated ion–molecule reactions. In addition, our results unravel the Takano *et al.* observation of ^{13}C isotopomers.[25] The authors discovered that the ^{13}C isotope is concentrated in the carbon atom of the HCC [13]CN molecule adjacent to the N atom. If ^{13}C is already enriched in [13]CN radicals, a reaction with $C_2H_2$ could propagate this isotope enrichment to the newly formed HCC [13]CN molecules.

Besides interstellar chemistry, the chemical dynamics of $CN(X\,^2\Sigma^+)$ radical reactions with unsaturated hydrocarbons are of fundamental relevance to the atmospheric chemistry in Saturn's moon Titan.[26] Titan's atmospheric composition is dominated by $N_2$ and $CH_4$ together with the minor components $C_2H_6$, $C_3H_8$, $C_2H_2$, HCN, $HC_3N$, $CH_3CCH$, and $C_2N_2$.[27,28] Its cyano chemistry is thought to be initiated by photolysis of HCN and $C_2N_2$ by solar radiation to generate reactive CN radicals in their $^2\Sigma^+$ electronic ground state. Upon the reaction with $C_2H_2$, the cyano radical can form then the experimentally detected HCCCN isomer cyanoacetylene. We would like to stress a fundamental difference between CN radical reactions in the interstellar medium (ISM) and planetary atmospheres. Due to the low density of only about $10^4$–$10^6$ molecules cm$^{-3}$ in molecular clouds in the ISM, only binary collisions are relevant; ternary processes do not play a role in the chemical processing of interstellar, cold molecular clouds. Therefore, the involved collision complexes HCCHCN and $H_2CCCN$ cannot be stabilized but decay to the HCCCN reaction products. In the denser planetary atmospheres, however, a third body collision can divert the internal energy to stabilize the HCCHCN and $H_2CCCN$ radicals together with potentially involved isonitrile intermediates. Therefore, chemical models of planetary atmospheres must include these highly reactive and photochemically active radical intermediates as well to give a consistent picture.

## VII. CONCLUSIONS

The chemical reaction dynamics to form cyanoacetylene, HCCCN $(X\,^1\Sigma^+)$, via the radical–neutral reaction of cyano radicals, $CN(X\,^2\Sigma^+;v=0)$, with acetylene, $C_2H_2(X\,^1\Sigma_g^+)$, are unraveled in crossed molecular beams experiments. The

reaction has no entrance barrier and is initiated by an attack of the CN radical to the $\pi$ electron density of the acetylene molecule to form a doublet cis/trans HCCHCN collision complex on the $^2A'$ surface via indirect reactive scattering dynamics. The four heavy atoms are rotating in the plane almost perpendicular to the total angular momentum vector **J** around the C axis of the complex. Here 85% of the collision complexes undergo C–H bond rupture through a tight transition state located 22 kJ mol$^{-1}$ above the cyanoacetylene, HCCCN $(X\,^1\Sigma^+)$ and H$(^2S_{1/2})$ products (microchannel 1). To a minor amount (15%) cis HCCHCN shows a 1,2 H shift via a 178 kJ mol$^{-1}$ barrier to form a doublet $H_2CCCN$ radical that is 46 kJ mol$^{-1}$ more stable than the initial reaction intermediate (microchannel 2). This $H_2CCCN$ complex decomposes via a rather loose exit transition state situated only 7 kJ mol$^{-1}$ above HCCCN $(X\,^1\Sigma^+)$ and H$(^2S_{1/2})$. The mild forward/sideways peaking of the center-of-mass angular distributions may well be related to the geometry of the relevant decomposing transition states within the microcanonical model of Roger Grice. The explicit identification of the cyanoacetylene as the only reaction product represents a solid background for the title reaction to be included in reaction networks modeling the chemistry in dark, molecular clouds, outflow of dying carbon stars, hot molecular cores, as well as the atmosphere of hydrocarbon-rich planets and satellites such as the Saturnian moon Titan.

[1] K. Fukuzawa and Y. Osamura, Astrophys. J. **489**, 113 (1997), and references therein.

[2] M. Ohishi and N. Kaifu, J. Chem. Soc. Faraday Discuss. **109**, 205 (1998).

[3] Y. Osamura, K. Fukuzawa, R. Terzieva, and E. Herbst, Astrophys. J. **519**, 697 (1999).

[4] I. Cherchneff and A. E. Glassgold, Astrophys. J. Lett. **419**, L41 (1993); T. J. Millar and E. Herbst, Astrophys. J. **288**, 561 (1994); S. D. Doty and C. M. Leung, *ibid.* **502**, 898 (1998); I. Cherchneff, A. E. Glassgold, and G. A. Mamon, *ibid.* **410**, 188 (1993).

[5] D. P. Ruffle *et al.*, Mon. Not. R. Astron. Soc. **291**, 235 (1997); T. J. Millar, G. H. Macdonald, and A. G. Gibbs, Astron. Astrophys. **325**, 1163 (1997).

[6] G. P. de Forets, D. R. Flower, and E. Herbst, Mon. Not. R. Astron. Soc. **253**, 359 (1991); E. Herbst *et al.*, *ibid.* **268**, 335 (1994); H. Suzuki *et al.*, Astrophys. J. **392**, 551 (1992).

[7] I. R. Sims *et al.*, Chem. Phys. Lett. **211**, 461 (1993); I. W. M. Smith, I. R. Sims, and B. R. Rowe, Chem. Eur. J. **3**, 1925 (1997).

[8] L. C. L. Huang, Y. T. Lee, and R. I. Kaiser, J. Chem. Phys. **110**, 7119 (1999).

[9] Y. T. Lee, J. D. McDonald, P. R. LeBreton, and D. R. Herschbach, Rev. Sci. Instrum. **40**, 1402 (1969).

[10] G. O. Brink, Rev. Sci. Instrum. **37**, 857 (1966); N. R. Daly, *ibid.* **31**, 264 (1960).

[11] M. S. Weis, Ph.D. thesis, University of California, Berkeley, 1986.

[12] A. D. Becke, J. Chem. Phys. **97**, 9173 (1992).

[13] C. Lee, W. Yang, and R. G. Parr, Phys. Rev. B **37**, 785 (1988).

[14] R. Krishnan, M. Frisch, and J. A. Pople, J. Chem. Phys. **72**, 4244 (1988).

[15] GAUSSIAN 98, Revision A.5, M. J. Frisch, G. W. Trucks, H. B. Schlegel *et al.*, Gaussian, Inc., Pittsburgh, PA, 1998.

[16] G. D. Purvis and R. J. Bartlett, J. Chem. Phys. **76**, 1910 (1982).

[17] H. Eyring, S. H. Lin, and S. M. Lin, *Basis Chemical Kinetics* (Wiley, New York, 1980).

[18] L. C. L. Huang, N. Balucani, Y. T. Lee, R. I. Kaiser, and Y. Osamura, J. Chem. Phys. **111**, 2857 (1999); N. Balucani, O. Asvany, A. H. H. Chang *et al.*, *ibid.* **111**, 7457 (1999); N. Balucani, O. Asvany, A. H. H. Chang *et al.*, *ibid.* **111**, 7472 (1999). For a compilation of all systems see http://po.iams.sinica.edu.tw/~kaiser

[19] R. Grice, Endeavour **17**, 173 (1993); R. Grice and D. J. Smith, Mol. Phys. **80**, 1533 (1993); D. J. Smith and R. Grice, *ibid.* **73**, 1371 (1991); N. W. Keane and R. Grice, *ibid.* **61**, 869 (1987).

[20] D. E. Woon and E. Herbst, Astrophys. J. **477**, 204 (1997).

[21] NIST database http://webbook.nist.gov/

[22] A. H. H. Chang, A. M. Mebel, X. M. Yang, S. H. Lin, and Y. T. Lee, J. Chem. Phys. **109**, 2748 (1998).

[23] M. Alagia, N. Balucani, P. Casavecchia, D. Stranges, and G. G. Volpi, J. Chem. Phys. **98**, 8341 (1993).

[24] F. Wyrowski, P. Schilke, and C. M. Walmsley, Astron. Astrophys. **341**, 882 (1999).

[25] S. Takano *et al.*, Astron. Astrophys. **329**, 1156 (1998).

[26] D. W. Clarke and J. P. Ferris, ''Origins of life and evolution of the biosphere 27,'' 1997, p. 225; ESA Special Publication SP-338, 1992, Symposium on Titan.

[27] B. Letourneur and A. Coustenis, Planet. Space Sci. **41**, 393 (1993).

[28] F. Raulin *et al.*, Adv. Space Res. **22**, 353 (1998).